A Predictive Model for the Elastic Properties of a Collagen-Hydroxyapatite Porous Scaffold for Multi-Layer Osteochondral Substitutes

Dario Gastaldi*, Gianluca Parisi, Riccardo Lucchini and Roberto Contro

Department of Chemistry Materials and Chemical Engineering
Politecnico di Milano, Piazza Leonardo da Vinci
32-20133 Milano, Italy
**dario.gastaldi@polimi.it*

Simone Bignozzi, Paola S. Ginestra, Giuseppe Filardo and Elisaveta Kon

Biomechanics Lab. II Clinic, Rizzoli Orthopaedic Institute
Via di Barbiano 1-10, Bologna, Italy

Pasquale Vena

Department of Chemistry Materials and Chemical Engineering
Politecnico di Milano, Piazza Leonardo da Vinci
32-20133 Milano, Italy

IRCCS Istituti Ortopedici Galeazzi, Milano, Italy

Received 18 February 2015
Revised 14 May 2015
Accepted 16 May 2015
Published 11 August 2015

Damaged articular cartilage can be substituted by porous scaffolds exhibiting tailored mechanical properties and with a suited layer-based design. Reliable predictive models are able to provide a structure–property relationship in the design phase is still an open issue which is of prominent relevance. In this paper, a bottom-up homogenization approach is presented having the purpose to determine the elastic properties of each single layer of a osteochondral porous three-layers scaffold: a top cartilage chondral layer and two mineralized layers: an intermediate and a subchondral bone layer. For the cartilage top layer, dry and wet conditions are considered; while, for intermediate and bone layers only dry conditions are considered. The homogenization model is based on the porosity of each layer and on the elastic properties of the constituent materials, i.e., water, hydroxyapatite (HA) and collagen. The elastic moduli predicted for the mineralized layers are compared with available literature results. The model results obtained on the cartilage layers are validated through flat punch micro-indentation tests carried out on wet and dry samples.

The results have shown that the elastic modulus of the mineralized layers is of the order of magnitude of few GPa; whereas, the elastic modulus of the cartilage layer which exhibits porosity higher than 90% is as low as 50 kPa and 300 kPa in wet and dry conditions, respectively. The above results show that the knowledge of the mechanical

*Corresponding author.

properties of the basic constituents which are universally known and the porosity of the layers are sufficient information to obtain a reliable prediction of the elastic properties of both mineralized layers and of cartilage layers.

1. Introduction

Tissue engineering has great potential in providing the appropriate replacement of diseased articular cartilage with a compatible substitute which is able to grant a reliable fixation into the joint defect and integration with the subchondral bone [Marcacci *et al.*, 2013a; Filardo *et al.*, 2014; Swieszkowski *et al.*, 2007]. The replaced engineered tissue, not only needs to be fully biocompatible with the individual subject in which it is implanted, but it also requires specific mechanical and structural properties for adequate functioning and integration within the body. One of the most widely adopted strategies relies on the use of an artificial structure, also regarded to as scaffolds, having the function of supporting stress under loading conditions and promoting the bio-mineralization process and the formation of new tissue. The resulting tissue constructs generally exhibit an overall composition that resembles that of the original tissue, but the tissue structure at nano and micro scales may be considerably different from that of the native tissue. This difference may compromise proper functionality and integration of the implants [Kelly and Prendergast, 2005].

The capability to reproduce the intrinsic gradient of properties in the osteochondral systems is a key point to grant mechanical compatibility with natural tissues and a proper biomechanical functionality. Mechanical integrity and adaptation to the different phases of implantation from the first to the mid and long term period is also of importance. To this purpose, multi-layer systems as those introduced in Tampieri *et al.* [2011a, 2011b], in Giannoni *et al.* [2012], in Lynn *et al.* [2010], Harley *et al.* [2010a, 2010b], and in Levingstone *et al.* [2014] are promising approaches to this problem.

In this work, an inhomogeneous monolithic scaffold is considered with three distinct layers, a chondral layer, an intermediate layer and a subchondral (bony) layer [Tampieri *et al.*, 2008]. Each of the three-layers is characterized by different constituents and architectural features in terms of average porosity. In particular, the chondral phase is the superficial layer composed by equine collagen; whereas, the intermediate layer (tide-mark) and the bony layer, are formed by a collagen/hydroxyapatite (HA) nanocomposite.

The capability to predict the mechanical properties of such multi-layer nanocomposite materials at the design stage as a function of the constituent properties, of the volume fractions as well as of shape and spatial organization at the nano and micro-scale level, is of great relevance for a knowledge-based approach to biomechanically compatible implant design.

In this paper, a homogenization model applied at multiple length scales is used to infer macroscopic mechanical properties of each single layer of the above described tissue substitute. The multiple scale hierarchical approach spans three scale levels: (i) the water/collagen compound (hydrated collagen) with bound water at nanometric scale level; (ii) the HA reinforced hydrated collagen and (iii) the large porosity at the tissue scale. Homogenization methods based on inclusions embedded in a matrix [Qu and Cherkaoui, 2007] was used at scale levels (i) and (ii); while, simplified structural models have been used at the tissue scale level. The results obtained through the homogenization models have been validated by making a comparison with available literature data on the calcified layers (the bottom layers which exhibit the highest elastic modulus). Furthermore, the results obtained on the chondral layer (the most compliant top layer) where compared with experimental results carried out on samples in dry and wet conditions.

2. Materials and Methods

2.1. *Layers description*

A commercial three layered scaffold (Maioregen; Fin-Ceramica S.p.A., Faenza, Italy) has been characterized in this study. An example of clinical application of the scaffold is reported in [Filardo *et al.*, 2013]. The chondral layer is the superficial layer composed by 100% deantigenated type I equine hydrated collagen. SEM images of the chondral layers [Tampieri *et al.*, 2008; Toni *et al.*, 2011] show a highly porous closed cell material with shell-like microstructure. The pores result more isotropic if compared with the mineralized composite and the average diameter was in the range of 100–150 μm [Tampieri *et al.*, 2008]. Cell walls are thinner than the struts thickness found in the mineralized layers and the porosity is higher than 90%.

The intermediate layer (tide-mark) and the subchondral layer instead, are formed by a randomly oriented network of collagen fibers with magnesium-enriched HA inclusions of different shapes exhibiting a trabecular-like microstructure. The Maioregen material has prescribed volume fractions of the constituents in the mineralized layers. In particular, the HA content in the tide-mark is 40 wt.% of the solid matrix; by accounting for the specific weight of HA crystals, it corresponds to 18% of volume fraction [Kon *et al.*, 2014]. The HA content in the subchondral layer is 70 wt.% of the solid matrix which corresponds to 48% volume fraction [Kon *et al.*, 2014]. The composite porosity of the tide-mark and the subchondral layers usually ranges between 80 and 85% and it is characterized by pores having the largest size ranging between 250 μm and 400 μm and a wall thickness of about 15–20 μm [Tampieri *et al.*, 2008, 2011a, 2011b].

2.2. *Multi-step homogenization models: Dry and wet conditions*

An estimate of the effective elastic properties of each layer has been obtained by means of a multi-step homogenization approach in which the layer is considered as

a nano/micro composite material with the specified material composition across the length scales. It is assumed that, at each length scale, the material can be considered as macroscopically homogeneous with micro-scale heterogeneities with known mechanical properties, spatial distribution and shapes. Under these hypotheses, a representative volume element (RVE) can be identified having characteristic length D. It is assumed that any RVE selected within the solid would exhibit the same mechanical property (i.e., effective stiffness). The characteristic length scale of the single heterogeneity d and that of the RVE (D) should be such that $D \gg d$ which represents the assumption of length scales separation in the homogenization process. The characteristic size at the largest length scale is that of the layer thickness which is assumed to be much smaller than D. With the exception of the largest length scale for which specific homogenization methods will be used, the homogenization steps involving the lower scale levels are based on the matrix-inclusions approach which makes use of the single inclusion problem solved by Eshelby [1957]. In each homogenization step, matrix and inclusions are identified and the properties of the matrix are obtained as the result of the homogenization problem solved for the previous scale level. In the following subsections, the multi-step homogenization approach is presented for the cartilaginous top layer; while the two mineralized layers (tide-mark and subchondral) are presented in a separate formulation with the purpose to account for their peculiar material constitution and the microstructural features of the porous structure.

2.2.1. *Cartilage layer*

Only two homogenization steps are involved in the cartilagineous-layer: (i) the smallest scale level for which water molecules are bound to dehydrated collagen particles forming the hydrated collagen solid structure and, (ii) the porous material in which the solid matrix is the hydrated collagen as obtained through the step (i). The effective properties of the hydrated collagen can be obtained by considering the dehydrated collagen particle immersed in a matrix the elastic properties of which are those of water. Isotropic properties for the dehydrated collagen have been assumed. The Young modulus and the Poisson ratio have been estimated from the components of the elastic tensor for the collagen as reported by Fritsch and Hellmich [2007]. The elastic modulus for the dehydrated collagen is obtained as the average values of elastic moduli along the three principal material directions ($E^{\mathrm{col}} = 9.5\,\mathrm{GPa}$); Poisson ratio has also been obtained as the average of Poisson ratios $\nu_{12}, \nu_{13}, \nu_{23}$ ($\nu^{\mathrm{col}} = 0.28$). The bounded water is assumed as an isotropic elastic solid with zero shear stiffness and bulk modulus $K_{H_2O} = 2.3\,\mathrm{GPa}$. The effective properties of the hydrated collagen ($\bar{\mathbf{L}}^{hc}$) is obtained through the self-consistent methods in which dehydrated collagen particles with volume fraction f_{col} are embedded in a isotropic matrix of bounded water molecules. The self-consistent scheme is an iterative scheme which provides the effective elastic tensor through a recursive relationship as reported in [Qu and Cherkaoui, 2007] and adapted with symbols

used in this work:

$$\bar{\mathbf{L}}^{hc} = \mathbf{L}^{H_2O} + f^{\text{col}}(\mathbf{L}^{\text{col}} - \mathbf{L}^{H_2O})\bar{\mathbf{T}}^{\text{col}}, \tag{1}$$

where

$$\bar{\mathbf{T}}^{\text{col}} = [\mathbf{I} + \mathbf{S}^{\text{col}}\bar{\mathbf{L}^{hc}}^{-1}(\mathbf{L}^{\text{col}} - \bar{\mathbf{L}}^{hc})]^{-1}. \tag{2}$$

In the above relationships, the elastic tensors of water and dry collagen are, respectively:

$$L^{H_2O}_{ijkl} = K^{H_2O}\delta_{ij}\delta_{kl}, \tag{3}$$

$$L^{\text{col}}_{ijkl} = K^{\text{col}}\delta_{ij}\delta_{kl} + \mu_{\text{col}}I^{d}_{ijkl}, \tag{4}$$

with $K^{\text{col}} = \frac{E^{\text{col}}}{3(1-2\nu^{\text{col}})}$, $\mu^{\text{col}} = \frac{E^{\text{col}}}{2(1+\nu^{\text{col}})}$ and $I^{d}_{ijkl} = (\delta_{ik}\delta_{jl} + \delta_{il}\delta_{jk} - \frac{2}{3}\delta_{ij}\delta_{kl})$.

In the above relationships, a simplifying assumption of spherical inclusions in a water-based matrix has been used; relevant limitations on the above assumption are mentioned in the discussion section.

The effective properties of the porous hydrated collagen is obtained through a further homogenization step. As a first attempt, the self-consistent method can be again used. In principle, low porosity solids ($\phi < 0.5$) being ϕ the porosity of the materials are correctly characterized by the self-consistent approach in which pores are clearly embedded in a hydrated collagen matrix. The solid matrix is characterized by the elastic tensor $\bar{\mathbf{L}}^{hc}$; while the pore can be considered as inclusions having vanishing stiffness. The effective elastic tensor for the cartilagineous layer $\bar{\mathbf{L}}^{\text{cart}}$ is therefore:

$$\bar{\mathbf{L}}^{\text{cart}} = \bar{\mathbf{L}}^{hc} + \phi(-\bar{\mathbf{L}}^{hc})\bar{\mathbf{T}}^{\text{pore}}, \tag{5}$$

where

$$\bar{\mathbf{T}}^{\text{pore}} = [\mathbf{I} + \mathbf{S}^{\text{pore}}\bar{\mathbf{L}}^{\text{cart}^{-1}}(-\bar{\mathbf{L}}^{\text{cart}})]^{-1} = [\mathbf{I} - \mathbf{S}^{\text{pore}}]^{-1}. \tag{6}$$

In the above expressions, $\mathbf{S}^{\text{col}}$ and $\mathbf{S}^{\text{pore}}$ are the Eshelby tensors for spherical inclusions in a homogeneous matrix having elastic tensors $\bar{\mathbf{L}}^{hc}$ and $\bar{\mathbf{L}}^{\text{cart}}$, respectively:

$$S^{c}_{ijkl} = \frac{5\nu^{c} - 1}{15(1-\nu^{c})}\delta_{ij}\delta_{kl} + \frac{4 - 5\nu^{c}}{15(1-\nu^{c})}(\delta_{ik}\delta_{jl} + \delta_{il}\delta_{jk}), \tag{7}$$

in which $c = \text{cart}, hc$ stands for cartilage and hydrated collagen, respectively.

Estimates of the effective elastic properties of highly porous structures with closed cells can be done by using finite element method on simplified models for cellular structures [Roberts and Garboczi, 2001]. The Effective Young modulus as function of the relative density of the material can be approximated for the high porosity range ($85\% < \phi < 90\%$) as:

$$E_{\text{cart}} = E_s 0.06(1-\phi)^{1.06}, \tag{8}$$

being E_s the Young modulus of the solid phase. The effective elastic modulus of the cartilagineous layer has been obtained in this work by means of the (8) and $E_s = E^{hc}$.

2.2.2. *Cartilage layer in wet conditions*

When the scaffold is immersed in fluid it swells, new water is bound to the solid matrix, the volume fraction of dry collagen in the solid phase as well as the porosity of the whole scaffold change. In the following, the estimate of the new porosity and the new volume fraction of dry collagen are obtained with the aim of determining the elastic properties of the wet scaffold. To this purpose, the water uptake (WU) as the ratio between the wet weight P^w and dry weight P^d of the three-layered sample are experimentally measured. The following assumptions are used: (i) new water is bound to the solid structure thus making the solid matrix more compliant than that exhibited in dry conditions; (ii) the volumetric swelling of the scaffold is homogeneous through all layers; (iii) all free water is taken out of the open pores before weighting the wet samples.

Under these assumptions, the relationship between the WU and the average volume swelling i.e., the ratio between the wet volume (V^w) and the dry volume (V^d) can be found as:

$$\mathrm{WU} = \frac{P^w}{P^d} = \frac{\gamma_w V_s^w}{\gamma_w V_s^{d-\mathrm{wet-col}}} = \frac{V_s^{d-\mathrm{wet-col}}(1+\epsilon_c)}{V_s^{d-\mathrm{wet-col}}} = 1+\epsilon_c, \tag{9}$$

in which $V^{d-\mathrm{wet-col}}$ is the volume occupied by the hydrated collagen component in the dry condition, V_s^w is the volume of the solid phase in wet conditions and WU is the WU experimentally measured. In the above equation, the assumption that specific weights of V_s^w and $V^{d-\mathrm{wet-col}}$ are approximately the same as that of water (γ_w) is made. This assumption is justified by the very high water content of the hydrated collagen in both dry and wet states. The total volume in wet conditions can be represented as:

$$V^w = \alpha V^d = (1 + B^{-1}\epsilon_c)V^d, \tag{10}$$

in which B is a volumetric strain localization factor which is the ratio between the volumetric strain due to swelling of the whole volume and the volumetric strain of the solid phase of the scaffold (ϵ_c).

Since only volumetric strains are assumed when the solid matrix swells in the wet condition, a scalar estimate of the strain localization factor for porous material with porosity ϕ^d can be obtained by summing all terms in the first three rows and three columns of the strain localization factor A_{ij} as defined in the Eshelby method:

$$B = \sum_{i,j=1}^{3} A_{ij}, \tag{11}$$

with

$$\mathbf{A} = \phi^d \bar{\mathbf{T}} + (1-\phi^d)\mathbf{I}, \tag{12}$$

in which $\mathbf{I}$ is the second-order identity tensor and $\bar{\mathbf{T}}$ is given by (6). From Eq. (9) the volumetric strain of the solid phase ϵ_c is:

$$\epsilon_c = \mathrm{WU} - 1. \tag{13}$$

The new volume fraction for hydrated collagen in wet condition $f^{\text{wet}-\text{col}}$ is:

$$f^{\text{wet}-\text{col}} = f^{\text{col}} \frac{1}{1+\epsilon_c}, \tag{14}$$

whereas, the porosity of the cartilage layer in wet condition ϕ^{wet} is $1 - f^{\text{wet}}$, this latter provided by Eq. (15):

$$f^{\text{wet}} = f^{d} \frac{1+\epsilon_c}{1+B^{-1}\epsilon_c}, \tag{15}$$

where f^{wet} and f^{d} are solid volume fraction of the sample in wet and dry conditions, respectively.

2.2.3. *Mineralized layers*

Three homogenization steps are involved in the characterization of the mineralized layers: (i) the smallest scale level for which water molecules are bound to dehydrated collagen particles forming the hydrated collagen solid structure, (ii) an intermediate scale level in which HA inclusions are bonded to the hydrated collagen matrix and (iii) the porous material in which the solid matrix is the nanocomposite hydrated collagen/HA as obtained through the step (ii). The elastic tensor for the solid matrix at homogenization level (ii), $\bar{\mathbf{L}}^{cH}$, is obtained by the self-consistent approach through the following implicit equation:

$$\bar{\mathbf{L}}^{cH} = \bar{\mathbf{L}}^{hc} + f^{Ha}(\mathbf{L}^{Ha} - \bar{\mathbf{L}}^{hc})\bar{\mathbf{T}}^{Ha}, \tag{16}$$

with

$$\bar{\mathbf{T}}^{Ha} = [\mathbf{I} + \mathbf{S}^{Ha}\bar{\mathbf{L}}^{cH-1}(\mathbf{L}^{Ha} - \bar{\mathbf{L}}^{cH})]^{-1}, \tag{17}$$

in which f^{Ha} is the volumetric fraction of HA particles. The components of the elastic tensor $\mathbf{L}^{Ha}$ for the HA particles are:

$$L^{Ha}_{ijkl} = K^{Ha}\delta_{ij}\delta_{kl} + \mu_{Ha} I^{d}_{ijkl}, \tag{18}$$

in which K^{Ha} and μ_{Ha} are bulk and shear modulus for the HA, respectively.

The Young modulus of the solid matrix E^{cH} is obtained through the compliance matrix $\bar{\mathbf{C}}^{cH} = \bar{\mathbf{L}}^{cH-1}$ as:

$$E^{cH} = \frac{1}{\bar{C}^{cH}_{11}}. \tag{19}$$

The third homogenization step provides the effective Young modulus of the porous layer. The mineralized layers exhibit a trabecular-like microstructure, therefore, an open cell structural model has been used [Zhu *et al.*, 1997] with the purpose to provide the elastic modulus of the porous mineralized layers ($E_{\text{min}-\text{layer}}$) as a function of the elastic modulus of the solid phase E_s and of the porosity as:

$$E_{\text{min}-\text{layer}} = CE^{cH}(1-\phi)^2, \tag{20}$$

in which $C = 0.63$ [Zhu *et al.*, 1997] and E^{cH} has been estimated by using Eq. (18); the properties of the intermediate layer (tide-mark) and of the subchondral layers are obtained by using $f^{Ha} = 0.18$ and $f^{Ha} = 0.44$, respectively.

2.3. *Experimental methods*

Unidirectional quasi-confined compression tests have been carried out on the cartilage layers of the samples. *Full three-layers scaffold have been tested*; *however*, *since shallow indentations are considered the mechanical characterization of the cartilage layer was not affected by the mineralized layers underneath.* All compressions where performed along the direction perpendicular to the articulating surface using two circular flat punches having radii of 250 μm and 500 μm. Scaffolds where tested in dry and wet conditions. The wet conditions were obtained by soaking the sample in a 22 wt.% water/glicerol mixture. Prior testing in wet conditions, excess water was removed by gentle shaking of the sample and WU was obtained by weighting the soaked samples. WU was obtained as the wet to dry weight ratio.

A custom fabricated micro-compression testing device has been used for all mechanical tests. A 5 N load cell (Honeywell, Model 31) was attached to a stepper motor (Physics Instruments) with displacement accuracy of 50 μm. LabView codes have been used to drive the stepper motor and to read synchronized signals from the motor and the load cell. The tests in wet conditions were performed by holding the samples in a liquid cell throughout the test.

The displacement-controlled tests were performed through a constant displacement rate (1 μm/sec) up to a maximum penetration depth of 70 μm. Once achieved the maximum displacement a holding time of 30 sec is applied before unloading at the same displacement rate. An estimation of the elastic modulus of the material has been obtained by making a linear interpolation the top part of the unloading force-displacement data, using the following relationship [Fischer-Cripps, 2007]:

$$E = \frac{dF}{du}\frac{1-\nu^2}{2R}, \tag{21}$$

in which $\frac{dF}{du}$ is the derivative of the applied force with respect to applied displacement calculated by means of a linear interpolation, ν is the Poisson ratio assumed as $\nu = 0.28$ and R is the radius of the circular flat indenter.

The effect of loading rate has been investigated by means of load-controlled micro-compression experiments performed by means of the NanoTest system (MicroMaterials, UK) by using a flat circular punch with radius of 500 μm. The tests were performed at a constant loading rates of $0.1, 0.5, 1, 2$ mN/sec. The elastic modulus of the samples at each loading rate has been estimated by applying (21).

3. Results

3.1. *Multi step homogenization models*

The elastic modulus of the hydrated collagen in the cartilage layer found through the self-consistent homogenization scheme decreases with the bound water content (see Fig. 1). For a water volume fraction of 99%, the Young modulus of the hydrated collagen was 67 MPa. The elastic modulus of the porous cartilage top layer as a function

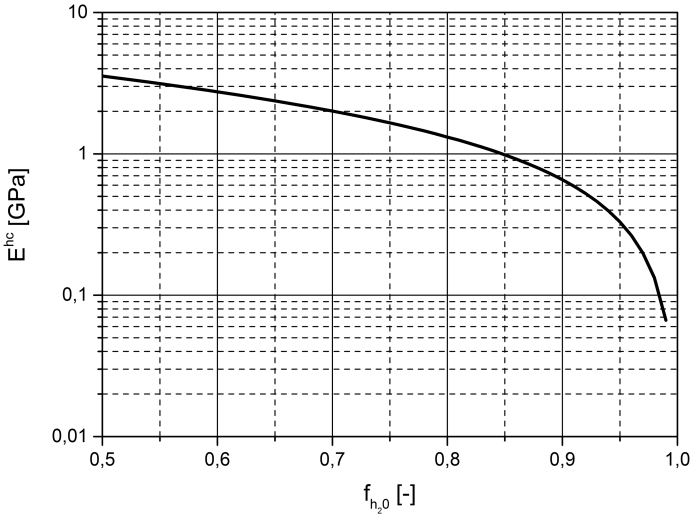

Fig. 1. Cartilage layer: Young modulus of Hydrated collagen versus water content.

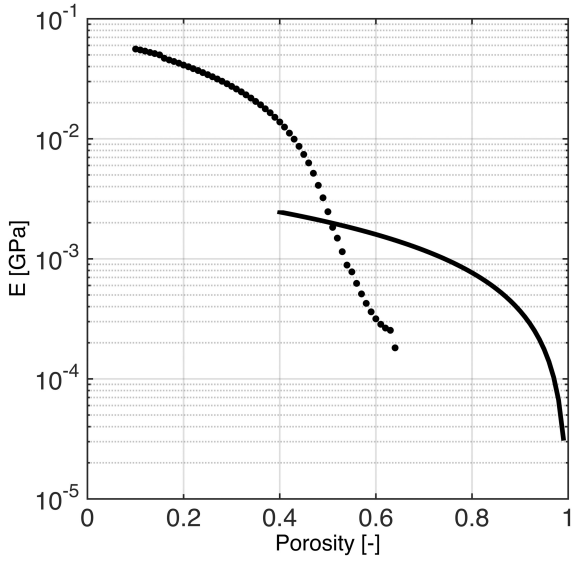

Fig. 2. Cartilage layer: Young modulus of the cartilage layer versus porosity as obtained through the self-consistent model (dashed line) and through the structural model of Eq. (8) (solid line).

of the layer porosity is shown in Fig. 2. As expected, the Young modulus decreases with the porosity. In Fig. 2, the result obtained through the self-consistent scheme is shown for porosity lower than 65%. For higher porosity, the results obtained through Eq. (8) are reported. The top cartilage layer is characterized by high porosity (up to 90% or more) for which the Young modulus of the porous structure is about 320 kPa.

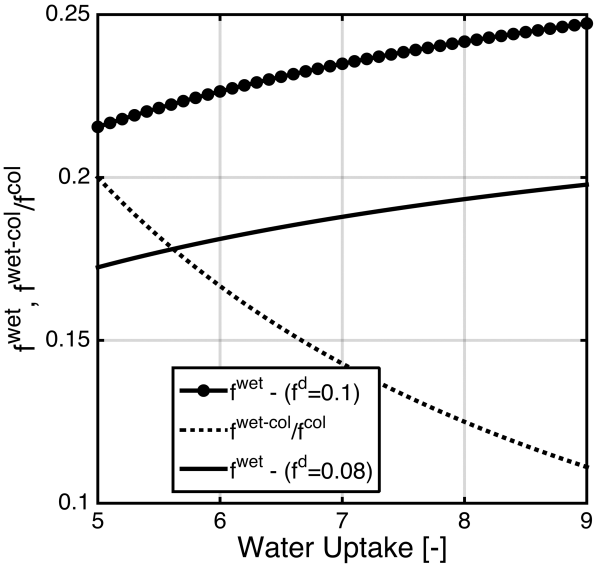

Fig. 3. Volume fraction of the solid phase in wet conditions for the cartilage layer f^{wet} and wet to dry ratio for collagen volume fractions ($\frac{f^{\mathrm{wet-col}}}{f^{\mathrm{ccol}}}$).

The WU measured experimentally was in the range 6–9; the collagen volume fraction in the hydrated collagen in wet condition ($f^{\mathrm{wet-col}}$) decreases with increasing WU. Under these conditions the parameter B^{-1} introduced in Eq. (10) as found by applying Eqs. (11) and (12) is 0.33. Figure 3 shows that $f^{\mathrm{wet-col}}$ for WU = 5 is 20% of f^{col} (the volume fraction of the collagen microstructure in dry condition) and it decreases to about 11% of f^{col} for WU = 9. The porosity of the cartilage layer generally decreases with WU, i.e., the wet solid fraction increases. Bold lines of Fig. 3 represent the volume fraction of the solid phase in wet conditions versus the WU for a dry solid fraction of 8% (92% porosity) and 10% (90% porosity). For the 10% dry solid fraction the wet solid fraction is 21.5% at WU = 5 and 25% at WU = 9. For the 8% dry solid fraction the wet solid fraction is 17% at WU = 6 and 20% at WU = 9.

Figure 4 shows the elastic modulus of the porous intermediate layer for the whole porosity range. In particular, the volume fraction of water is 52% and the volume fraction of HA is 18%. For porosity lower than 40%, the self-consistent scheme has been used; while, the structural model (19) has been used for higher porosity. At 85% porosity, a Young modulus of 100 MPa has been found. The elastic properties of the subchondral layer were estimated with a water volume fraction of 52% and HA volume fraction of 44%. Figure 5 shows the estimates for the elastic modulus of the subchondral layer as obtained through the self-consistent scheme and through the structural model (19). The bullets represent the experimental measure of the elastic

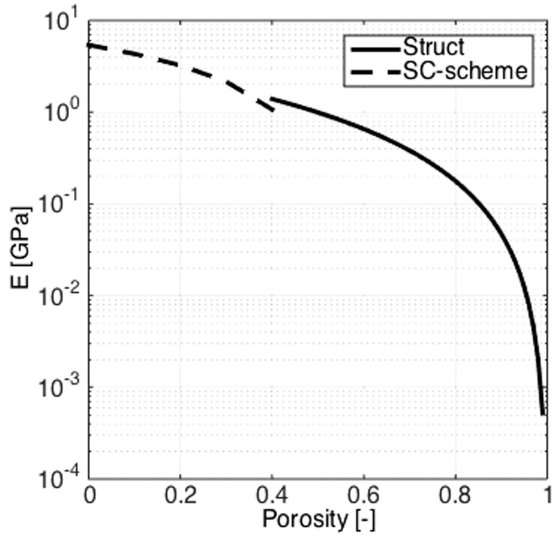

Fig. 4. Intermediate layer: Young modulus as a function of the layer porosity.

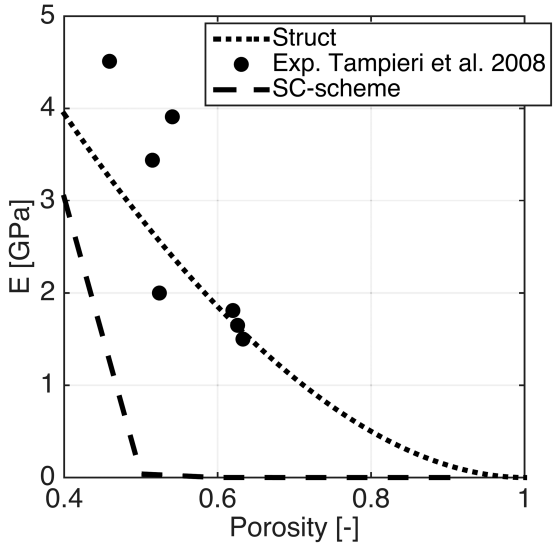

Fig. 5. Young modulus of the subchondral layer: Self-consistent scheme (dashed line), structural model (dotted line). Bullets represents experimental results as found by Tampieri *et al.* [2011a].

modulus as obtained by Landi *et al.* in [Landi *et al.*, 2008]. Figure 5 shows that the experimental elastic modulus of the porous subchondral layer is well represented by the structural model, while self-consistent scheme underestimated the elastic modulus.

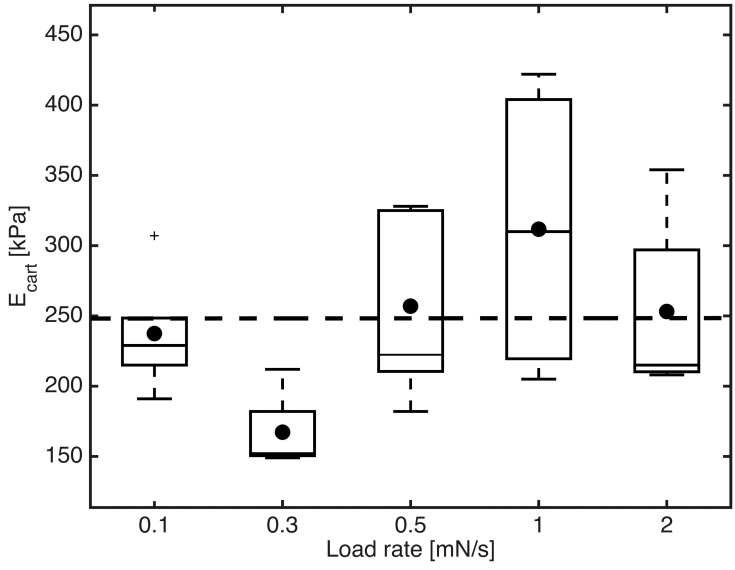

Fig. 6. Box plot from compression of the dry cartilage layer: elastic modulus at different loading rates. Bullets represent average values, bars in the box are median values.

3.2. *Micro-compression experiments*

Although the experiments were performed on the three-layers scaffolds, the penetration depths was shallow (less than 70 μm) with respect to the layer thickness; therefore it is assumed that the results presented in this sections are relevant for the top cartilage layer only.

The effect of loading rate is shown in the box plot of Fig. 6. The filled circles represent the average elastic moduli at each load rate; while the top and bottom bounds of the boxes represent the 95% and 5% of all experimental measures. Top and bottom whiskers represent the extreme measured values. Outiers are reported with cross symbols. An average elastic modulus computed on all loading rates is 250 kPa in dry conditions and no explicit effect of loading rates was observed for the specific loading protocol. Figure 7 shows the elastic moduli estimated using the 0.5 mm and 1 mm punch diameters, no significant difference was found between the two groups of measures; an average elastic modulus of 300 kPa was found. The experiments performed on the three-layers scaffold in wet conditions resulted in lower elastic modulus for the cartilage porous layer. Figure 8 shows the box plots for two sets of measures with WU = 5.6 and WU = 8.9, respectively. An average value elastic modulus of dry three-layers scaffolds is also reported. The symbols reported in Fig. 8 represent the analytical estimates obtained for wet samples by selecting the relevant WU values and dry solid fractions of 8% (stars) and 10% (black squares). The analytical model estimates a decreasing elastic model with an increasing WU and the analytical elastic modulus for the dry scaffold is larger

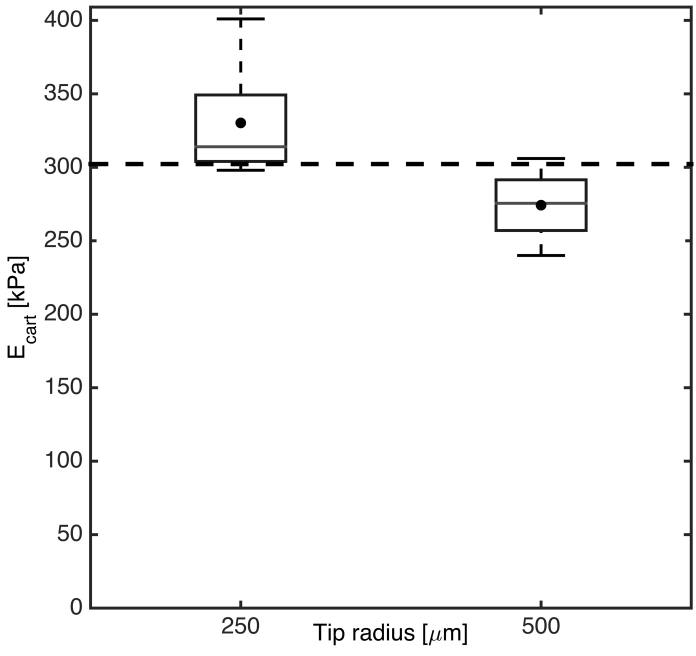

Fig. 7. Box plot from compression of the dry cartilage layer: elastic modulus of the scaffold at the two tip radii. Bullets represent average values, bars in the box are median values. An average value of 300 KPa was found (bold dashed line).

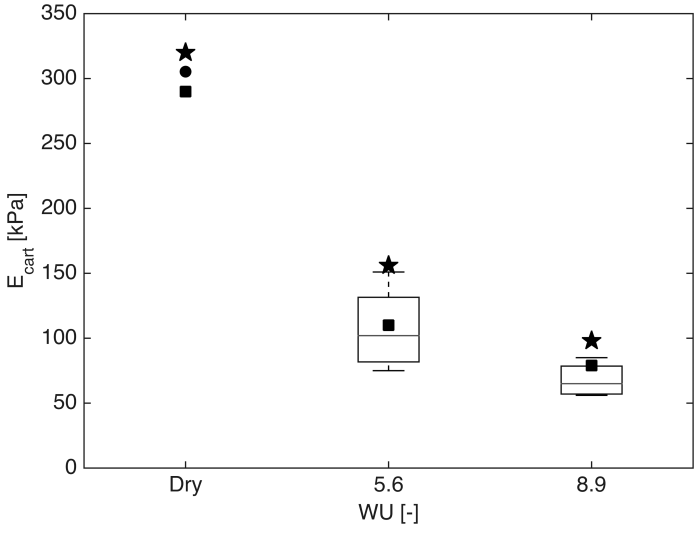

Fig. 8. Box plots from compression of wet cartilage layer at two different WU values. The average result obtained with tests in dry conditions is also reported. Stars and filled squares symbols represent model predictions at solid volume fraction of 10% and 8%, respectively, bars in the box are median values, the bullet represents the average experimental estimation for dry cartilage.

than those found for the wet samples; these findings are consistent with those found experimentally. A systematic over-estimation of the analytical estimates for 10% dry solid fraction has been found; the largest over-estimation has been found for WU = 5.6 of about 50%; while, analytical estimates obtained with the 8% dry solid fraction are in good agreement with the experimental measures for both dry and wet conditions.

4. Discussion

The clinical and scientific relevance of the tissue engineering approach to osteochondral defect treatment is undisputed. However, the achievement of a functional scaffold material able to grant primary mechanical stability, biomechanical compatibility and effective tissue repair relies on several different aspects, including mechanical properties. The approaches used in Tampieri *et al.* [2011a, 2011b], in Giannoni *et al.* [2012], in Lynn *et al.* [2010], and in Harley *et al.* [2010a, 2010b] introduce multi-layer systems which exhibit biomechanically compatible composite components with a graded material stiffness able to minimize stiffness mismatch between the hosted material and the surrounding tissues.

Mechanical properties of the multi-layer scaffold are often characterized *a posteriori* by means of mechanical laboratory tests [Harley *et al.*, 2007].

This leads to the need of models able to predict the mechanical properties of osteochondral scaffolds *a priori* by means of bottom-up approaches which rely on the knowledge of the mechanical properties of the fundamental building blocks of the scaffold. In particular, this paper presents a bottom-up model aimed at predicting the elastic properties of a multi-layer porous scaffold for ostechondral substitutes in dry and wet conditions. In particular, the elastic modulus of the three-layers of collagen/HA nanocomposite porous structures has been obtained by making use of homogenization approaches as well as simplified structural models.

The following layers have been characterized: a full collagenous cartilage layer, a 18% volume fraction of HA as intermediate layer and a 44% volume fraction HA as subchondral layer. The analytical estimates have been compared with literature data on the subchondral layer and with experimental data for the top cartilage layer. To this purpose dry and wet samples have been tested by flat punch compression experiments.

The proposed bottom-up hierarchical model considers three scale levels: (i) the hydrated collagen with bound water at the nanometric scale level; (ii) the HA reinforced hydrated collagen and (iii) the large porosity at the tissue scale. The self-consistent homogenization schemes based on the Eshelby single inclusion model have been used for the nanoscale levels, i.e., level (i) and (ii); whereas, open and closed cell structural models have been used for the highly porous scaffolds at the tissue level. The elastic properties of the basic building blocks have been used at the nanoscale, i.e., bound water, collagen particles and HA crystals as starting

points of this multi-scale bottom-up approach. Eshelby-based methods have been largely used in the nano and microscale mechanics of bone tissue as proposed in [Fritsch and Hellmich, 2007] and in [Hellmich *et al.*, 2004]; however no applications on collagen-based tissue engineering scaffold for osteochondral substitute was found. *The predictive capability of this model is discussed in the following.* The elastic moduli obtained for the subchondral layer have been found in very good agreement with the experimental results presented in Tampieri *et al.* [2008].

The elastic modulus of the cartilage layer was compared with experimental data obtained by flat punch compression tests; dry and wet conditions were analyzed. Very good agreement with experimental data was found for the layer porosity model parameter of 0.92. An over-estimation of the elastic modulus was found for porosity of 0.9, instead.

The wet conditions were estimated by measuring the WU of the samples and estimating the collagen volume fractions at the nanoscale for the wet material. As expected a decreasing elastic modulus was found for increasing WU; the elastic modulus was as low as approximately 100 kPa for a WU equal to 8.9.

Previous papers have dealt with the characterization of porous scaffold materials, but very few contributions focuses on the mechanical characterization with special reference to cartilage scaffold. Zhang *et al.* [2014] investigated the effect of pore size and porosity on the elastic properties of the scaffold under compression tests. They found an elastic modulus as low as 20 KPa for scaffolds having a pore size range 150–250 μm and 98.8% porosity; the elastic moduli found in our study are of the same order of magnitude although slightly higher than those found in Zhang *et al.* as porosity of 92% was considered in our study.

In Harley *et al.* [2007] collagen-based scaffold in dry and wet conditions have been mechanically characterized; mechanical characterization on the single struts were also performed. Harley *et al.* found an elastic modulus of the individual scaffold struts as low as 5 MPa, this value is consistent with the wet collage-water nanocomosite found in this study to be between 7 MPa and 12 MPa for WU of 9 and 5, respectively. The elastic modulus of the dry collagen-based strut measured in [Harley *et al.*, 2007] was 762 MPa which is higher than that found in this study (67 MPa) for a 99% volume fraction of water. The value of 762 MPa would be consistent with a 87% volume fraction of water.

The above discussion reveals that the results found in this study are consistent with the existing literature; however some limitations are identified and discussed in the following. No experimental data on tide-mark were available, therefore validation of the model for that specific layer was not achieved. This lack of validation has a limited relevance as the validation of the most compliant and of the stiffest layer have been successfully achieved.

It must be underlined that the intermediate layer is thinner than the top and bottom layers, being it less than 1 mm thick. This limits the suitability of the homogenization approach for this specific layer. Indeed, while the thickness of the cartilage

and subchondral layers are at least one order of magnitude larger than the expected pore size; this is not the case for the intermediate layer. This would imply that the scale separation required for reliable homogenization approaches is met for the top and bottom layers, while it is critical for the intermediate layer.

The hydrated collagen is obtained starting from equine collagen. Actual nanostructure of the collagen/water system is not available, therefore the modeling of this system through the inclusion in a matrix approach with spherical particles is a simplified assumption; inclusions in the models are not necessarily related to the actual shape of dry collagen particles. At the nanoscale, the hydrated collagen is the result of a self-assembling process of collagen fibrils in which a staggered arrangement of parallel molecules is formed. This would suggest anisotropic mechanical properties, which has not been taken into consideration in this work. We believe that this assumption has a limited effect on the overall mechanical behavior of the scaffold at the macroscopic scale. Furthermore, Peculiar geometry of pores and direction-dependent porosity may give anisotropic material response at the macro scale. This has been neglected for lack of specific information on directional porosity or on specific geometry of HA inclusions. Therefore, only Young modulus of an effective isotropic material model at all levels was investigated. A more comprehensive approach making use of computer tomography imaging data may be used to this specific purpose [Lynn *et al.*, 2010; Scheiner *et al.*, 2009].

Buckling of the tiny microstructure occurring upon compressive loading [Gibson, 2005] was not modeled as only moderate compressive stress was applied on the experimental compression tests and the plateau on the stress–strain plot, which is typical of buckling upon compression, was not observed.

Lastly, the effect of the cross linking agents used in the manufacturing process to create hydrated collagen matrix was not quantitatively introduced in the homogenization model. In [Tampieri *et al.*, 2008] a higher number of links between the collagen bundles in the cross-linked samples with respect to noncross linked samples has been shown. This has an effect on the mechanical response of the cartilage layer which was not quantified in the present work. In order to do this, a quantitative estimation of the effect of the cross linking agent on the architectural changes of the microstructure would be required.

Clinical studies of such devices have already proven that such materials are an emerging and promising technology for knee cartilage regeneration [Marcacci *et al.*, 2013a]. A comprehensive characterization of such materials including their mechanical response is crucial for a successful clinical application.

In this paper, the mechanical characterization of multi-layer osteochondral scaffold has been carried out proving that homogenization approaches applied at multiple scale level can effectively predict mechanical properties of the tissue substitute in dry as well as in clinically relevant wet conditions; thus providing a suitable tool for a knowledge-based design of innovative collagen-based nanocomposites for biocompatible implantable devices.

References

Eshelby, J. D. [1957] "The determination of elastic field of an ellipsoidal inclusion, and related problems," *Proceedings of the Royal Society London A* **241**, 376–396.

Filardo, G., Drobnic, M., Perdisa, F., Kon, E., Hribernik, M. and Marcacci, M. [2014] "Fibrin glue improves osteochondral scaffold fixation: Study on the human cadaveric knee exposed to continuous passive motion," *Osteoarthritis Cartilage* **22**(4), 557–565.

Filardo, G., Kon, E., Di Martino, A., Busacca, M., Altadonna, G. and Marcacci, M. [2013] "Treatment of knee osteochondritis dissecans with a cell-free biomimetic osteochondral scaffold clinical and imaging evaluation at 2-year follow-up," *The American Journal fo Sports Medicine* **41**(8), 1786–1793.

Fischer-Cripps, A. C. [2007] *Introduction to Contact Mechanics* (Springer, New York, USA).

Fritsch, A. and Hellmich, C. [2007] "'Universal' microstructural patterns in cortical and trabecular, extracellular and extravascular bone materials: Micromechanics-based prediction of anisotropic elasticity," *Journal of Theoretical Biology* **244**(4), 597–620.

Giannoni, P., Lazzarini, E., Ceseracciu, L., Barone, A., Quarto, R. and Scaglione, S. [2012] "Design and characterization of a tissue-engineered bilayer scaffold for osteochondral tissue repair," *Journal of Tissue Engineering and Regenerative Medicine*, doi: 10.1002/term.1651

Gibson, L. J. [2005] "Biomechanics of cellular solids," *Journal of Biomechanics* **38**, 377–399.

Harley, B. A., Leung, J. H., Silva, E. C. C. M. and Gibson, L. J. [2007] "Mechanical characterization of collagen-glycosaminoglycan scaffolds," *Acta Biomaterialia* **3**(4), 463–474.

Harley, B. A., Lynn, A. K., Wissner-Gross, Z., Bonfield, W., Yannas, I. V. and Gibson, L. J. [2010a] "Design of a multiphase osteochondral scaffold. III. Fabrication of layered scaffolds with continuous interfaces," *Journal of Biomedical Materials and Research Part A* **92A**(3), 1078–1093.

Harley, B. A., Lynn, A. K., Wissner-Gross, Z., Bonfield, W., Yannas, I. V. and Gibson, L. J. [2010b] "Design of a multiphase osteochondral scaffold. II. Fabrication of a mineralized collagen-glycosaminoglycan scaffold," *Journal of Biomedical Materials and Research Part A* **92A**(3), 1066–1077.

Hellmich, C., Barthelemy, J. F. and Dormieux, L. [2004] "Mineral-collagen interactions in elasticity of bone ultrastructure — A continuum micromechanics approach," *European Journal of Mechanixs A-Solids* **23**(5), 783–810.

Kelly, D. J. and Prendergast, P. J. [2005] "Mechano-regulation of stem cell differentiation and tissue regeneration in osteochondral defects," *Journal of Biomechanics* **38**(7), 1413–1422.

Kon, E., Filardo, G., Perdisa, F., Venieri, G. and Marcacci, M. [2014] "Clinical results of multilayered biomaterials for osteochondral regeneration," *Journal of Experimental Orthopaedic*, **1**, 10.

Landi, E., Valentini, F. and Tampieri, A. [2008] "Porous hydroxyapatite/gelatine scaffolds with ice-designed channel-like porosity for biomedical applications," *Acta Biomaterialia* **4**(6), 1620–1626.

Levingstone, T. J., Matsiko, A., Dickson, G. R., O'Brien, F. J. and Gleeson, J. P. [2014] "A biomimetic multi-layered collagen-based scaffold for osteochondral repair," *Acta Biomaterialia* **10**(5), 1996–2004.

Lynn, A. K., Best, S. M., Cameron, R. E., Harley, B. A., Yannas, I. V., Gibson, L. J. and Bonfield, W. [2010] "Design of a multiphase osteochondral scaffold. I. Control of

chemical composition," *Journal of Biomedical Materials and Research Part A* **92A**(3), 1057–1065.

Marcacci, M., Zaffagnini, S., Kon, E., Marcheggiani Muccioli, G. M., Di Martino, A., Di Matteo, B., Bonanzinga, T., Iacono, F. and Filardo, G. [2013a] "Unicompartmental osteoarthritis: An integrated biomechanical and biological approach as alternative to metal resurfacing," *Knee Surgery, Sports Traumatology, Arthroscopy* **21**(11), 2509–2517.

Marcacci, M., Filardo, G. and Kon, E. [2013b] "Treatment of cartilage lesions: What works and why?" *Injury* **44**(1), S11–S15.

Qu, J. and Cherkaoui, M. [2007] *Fundamentals of Micromechanics* (John Wiley & Sons, Hoboken, New Jersey).

Roberts, A. P. and Garboczi, E. J. [2001] "Elastic moduli of model random three-dimensional closed-cell cellular solids," *Acta Materialia* **49**(2), 189–197.

Scheiner, S., Sinibaldi, R., Pichler, B., Komlev, V., Renghini, C., Vitale-Brovarone, C., Rustichelli, F. and Hellmich, C. [2009] "Micromechanics of bone tissue-engineering scaffolds, based on resolution error-cleared computer tomography," *Biomaterials* **30**(12), 2411–2419.

Swieszkowski, W., Tuan, B. H. S., Kurzydlowski, K. J. and Hutmacher, D. W. [2007] "Repair and regeneration of osteochondral defects in the articular joints," *Biomolecular Engineering* **24**(5), 489–495.

Tampieri, A., Sandri, M., Landi, E., Pressato, D., Francioli, S., Quarto, R. and Martin, I. [2008] "Design of graded biomimetic osteochondral composite scaffolds," *Biomaterials* **29**(26), 3539–3546.

Tampieri, A., Sprio, S., Sandri, M. and Valentini, F. [2011a] "Mimicking natural bio-mineralization processes: A new tool for osteochondral scaffold development," *Trends in Biotechnology* **29**(10), 526–535.

Tampieri, A., Landi, E., Valentini, F., Sandri, M., D'Alessandro, T., Dediu, V. and Marcacci, M. [2011b] "A conceptually new type of bio-hybrid scaffold for bone regeneration," *Nanotechnology* **22**(1), 015104.

Toni, R., Tampieri, A., Zini, N., Strusi, V., Sandri, M., Dallatana, D., Spaletta, G., Bassoli, E., Gatto, A., Ferrari, A. and Martin, I. [2011] "Ex situ bioengineering of bioartificial endocrine glands: A new frontier in regenerative medicine of soft tissue organs," *Annals of Anatomy* **193**(5), 381–394.

Zhang, Q., Lu, H., Kawazoe, N. and Chen, G. [2014] "Pore size effect of collagen scaffolds on cartilage regeneration," *Acta Biomaterialia* **10**(5), 2005–2013.

Zhu, H. X., Knott, J. F. and Mills, N. J. [1997] "Analysis of the elastic properties of open-cell foams with tetrakaidecahedral cells," *Journal of the Mechanics and Physics of Solids* **45**(3), 319–343.